A time domain numerical method for the low frequency Biot model

Guillaume Chiavassa, Bruno Lombard, Joel Piraux

10ème **C**ongrès **F**rançais d'**A**coustique

Lyon, 12-16 Avril 2010

A Time Domain Numerical Method for the low frequency Biot model

Guillaume Chiavassa[1], Bruno Lombard[2], Joël Piraux[2]

[1] Ecole Centrale Marseille et M2P2, Technopôle de Château-Gombert, 13451 Marseille, guillaume.chiavassa@centrale-marseille.fr

[2] Laboratoire de Mécanique et d'Acoustique, 31 ch. Joseph Aiguier, 13402 Marseille, {lombard,piraux}@lma.cnrs-mrs.fr

A numerical method is proposed to simulate the propagation of transient poroelastic waves across 2D heterogeneous media, in the low frequency range. A velocity-stress formulation of Biot's equations is followed, leading to a first-order system of partial differential equations. This system is splitted in two parts: a propagative one discretized by a fourth-order ADER scheme, and a diffusive one that is solved analytically. Near material interfaces, a space-time mesh refinement is implemented to capture the small spatial scales related to the slow compressional wave. Lastly, an immersed interface method is implemented to accurately model the jump conditions between the different media and the geometry of the interfaces. Numerical experiments and comparisons with exact solutions confirm the efficiency and the accuracy of the approach.

1 Introduction

The propagation of poroelastic waves is of interest in many areas of applied mechanics, including industrial foams, spongious bones and petroleum rocks. The most-widely-used model describing the evolution of mechanical perturbations in a saturated porous medium was proposed by Biot in 1956. Two regimes were distinguished by Biot: one corresponding to a low-frequency range [2], and one to a high-frequency range, where some of the physical parameters depend on the frequency [3]. We focus on transient mechanical waves whose frequency content lies in the low-frequency range.

Until the mid 1990's, Biot's equations were mainly studied in the harmonic regime. Various time-domain methods have been proposed since, based on finite-differences [6, 18], finite-elements [19], boundary-elements [16], and spectral methods. Since non-realistic values of the physical parameters were used, the real difficulties arising when performing time-domain simulations were often overlooked. These difficulties are induced by the coexistence of solutions with radically different dynamics: propagating "fast" compressional wave and shear wave on one hand, and a diffusive "slow" compressional wave on the other hand [4]. The latter is highly dispersed and attenuated when the saturating fluid is viscous, and then remains localized near sources and interfaces.

The aim of the present study is to develop an efficient numerical strategy to compute the solution made up of the whole wave field. A time-splitting is used together with a fourth-order ADER scheme [17]. A flux-conserving space-time mesh refinement is implemented around the interfaces [1]. Lastly, an immersed interface method gives a subcell resolution of the interfaces and accurately enforces the jump conditions between different porous media [12, 13].

This paper generalizes to two-dimensional configurations a preliminary 1D work [5]. It is organized as follows. The Biot's model is briefly recalled in section 2. The numerical methods are described in section 3. Section 4 presents numerical experiments of interaction between a plane wave and 1 or 3 cylinders. In section 5, conclusions are drawn and some future perspectives are suggested.

2 Physical modeling

2.1 Configuration

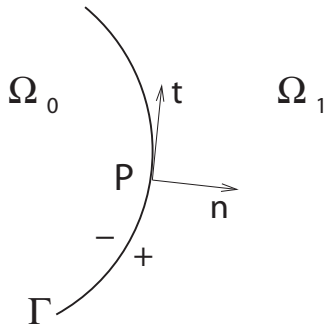

Figure 1: Interface Γ between two media Ω_0 and Ω_1.

Let us consider a two-dimensional configuration with two poroelastic media Ω_0 and Ω_1, separated by a stationary interface Γ (figure 1). This interface is assumed to be sufficiently smooth in order to be differentiated as many times as required by the immersed interface method. At any point P on Γ, the tangential and normal vectors are respectively denoted by $\mathbf{t}$ and $\mathbf{n}$.

2.2 Biot's model

The Biot's model involves 10 physical parameters: the density ρ_f and the dynamic viscosity η of the fluid; the density ρ_s and the shear modulus μ of the solid skeleton;

the porosity $0 < \phi < 1$, the tortuosity $a \geq 1$, the absolute permeability κ, the Lamé coefficient λ_f and the two Biot's coefficients β and m of the saturated matrix. The following notations are introduced: $\rho_w = \frac{a}{\phi}\rho_f$, $\rho = \phi\,\rho_f + (1-\phi)\,\rho_s$, and $\chi = \rho\,\rho_w - \rho_f^2 > 0$. The unknowns are the elastic velocity $\mathbf{v}_s$, the filtration velocity $\mathbf{w} = \phi\,(\mathbf{v}_f - \mathbf{v}_s)$ where $\mathbf{v}_f$ is the acoustic velocity, the independant components of the elastic stress tensor σ, and the acoustic pressure p. In 2D, it amounts to 8 unknowns.

The physical parameters are piecewise constant and discontinuous across Γ. In the case of perfect bonded contact between the two media, the jump conditions along Γ are

$$\begin{aligned} &[\mathbf{v}_s.\mathbf{n}] = 0, \quad [\mathbf{v}_s.\mathbf{t}] = 0, \quad [\mathbf{w}.\mathbf{n}] = 0, \\ &[(\sigma.\mathbf{n})\,.\,\mathbf{n}] = 0, \quad [(\sigma.\mathbf{n})\,.\,\mathbf{t}] = 0, \quad [p] = 0. \end{aligned} \tag{1}$$

We assume that the spectrum of the source lies mainly in the low-frequency range, involving frequencies lower than

$$f_c = \frac{\eta\,\phi}{2\,\pi\,a\,\kappa\,\rho_f}. \tag{2}$$

Consequently, no frequential correction of the viscosity is required [2, 4], leading to the following velocity-stress evolutionary equations

$$\begin{aligned} &\frac{\partial\,v_{s1}}{\partial\,t} - \frac{\rho_w}{\chi}\left(\frac{\partial\,\sigma_{11}}{\partial\,x} + \frac{\partial\,\sigma_{12}}{\partial\,y}\right) - \frac{\rho_f}{\chi}\,\frac{\partial\,p}{\partial\,x} = \frac{\rho_f}{\chi}\,\frac{\eta}{\kappa}\,w_1, \\ &\frac{\partial\,v_{s2}}{\partial\,t} - \frac{\rho_w}{\chi}\left(\frac{\partial\,\sigma_{12}}{\partial\,x} + \frac{\partial\,\sigma_{22}}{\partial\,y}\right) - \frac{\rho_f}{\chi}\,\frac{\partial\,p}{\partial\,y} = \frac{\rho_f}{\chi}\,\frac{\eta}{\kappa}\,w_2, \\ &\frac{\partial\,w_1}{\partial\,t} + \frac{\rho_f}{\chi}\left(\frac{\partial\,\sigma_{11}}{\partial\,x} + \frac{\partial\,\sigma_{12}}{\partial\,y}\right) + \frac{\rho}{\chi}\,\frac{\partial\,p}{\partial\,x} = -\frac{\rho}{\chi}\,\frac{\eta}{\kappa}\,w_1, \\ &\frac{\partial\,w_2}{\partial\,t} + \frac{\rho_f}{\chi}\left(\frac{\partial\,\sigma_{12}}{\partial\,x} + \frac{\partial\,\sigma_{22}}{\partial\,y}\right) + \frac{\rho}{\chi}\,\frac{\partial\,p}{\partial\,y} = -\frac{\rho}{\chi}\,\frac{\eta}{\kappa}\,w_2, \\ &\frac{\partial\,\sigma_{11}}{\partial\,t} - (\lambda_f + 2\,\mu)\,\frac{\partial\,v_{s1}}{\partial\,x} - \beta\,m\,\frac{\partial\,w_1}{\partial\,x} - \lambda_f\,\frac{\partial\,v_{s2}}{\partial\,y} \\ &\qquad -\beta\,m\,\frac{\partial\,w_2}{\partial\,y} = 0, \\ &\frac{\partial\,\sigma_{12}}{\partial\,t} - \mu\left(\frac{\partial\,v_{s2}}{\partial\,x} + \frac{\partial\,v_{s1}}{\partial\,y}\right) = 0, \\ &\frac{\partial\,\sigma_{22}}{\partial\,t} - \lambda_f\,\frac{\partial\,v_{s1}}{\partial\,x} - \beta\,m\,\frac{\partial\,w_1}{\partial\,x} - (\lambda_f + 2\,\mu)\,\frac{\partial\,v_{s2}}{\partial\,y} \\ &\qquad -\beta\,m\,\frac{\partial\,w_2}{\partial\,y} = 0, \\ &\frac{\partial\,p}{\partial\,t} + m\left(\beta\,\frac{\partial\,v_{s1}}{\partial\,x} + \frac{\partial\,w_1}{\partial\,x} + \beta\,\frac{\partial\,v_{s2}}{\partial\,y} + \frac{\partial\,w_2}{\partial\,y}\right) = 0. \end{aligned} \tag{3}$$

Setting

$$\mathbf{U} = (v_{s1},\, v_{s2},\, w_1,\, w_2,\, \sigma_{11},\, \sigma_{12},\, \sigma_{22},\, p)^T,$$

one writes (3) as a first-order linear system

$$\frac{\partial}{\partial\,t}\,\mathbf{U} + \mathbf{A}\,\frac{\partial}{\partial\,x}\,\mathbf{U} + \mathbf{B}\,\frac{\partial}{\partial\,y}\,\mathbf{U} = -\mathbf{S}\,\mathbf{U}, \tag{4}$$

where $\mathbf{A}$, $\mathbf{B}$ and $\mathbf{S}$ are 8×8 matrices.

2.3 Properties

A detailed mathematical analysis of (4) is proposed in [7]: existence, uniqueness and smoothness of the solutions. Here we focus on the properties useful for numerical modeling. The spectral radius of $\mathbf{S}$ is $R(\mathbf{S}) = \frac{\eta}{\kappa}\,\frac{\rho}{\chi}$, with typical values $R(\mathbf{S}) \approx 10^6$: the system (4) is *stiff*.

The eigenvalues of $\mathbf{A}$ and $\mathbf{B}$ are real: $\pm\overline{c}_{p1}$, $\pm\overline{c}_{p2}$, $\pm\overline{c}_s$, and 0 (multiplicity 2), with $\overline{c}_{p1} > \overline{c}_s > \overline{c}_{p2} > 0$. The waves associated with $\overline{c}_{p1}$ and $\overline{c}_{p2}$ are compressional waves, respectively called *fast wave* and *slow wave*; usually, one gets $\overline{c}_{p2} \ll \overline{c}_{p1}$. The wave associated with $\overline{c}_s$ is a shear wave. A dispersion analysis of (3) provides the phase velocities $c_{p1}(f)$, $c_{p2}(f)$ and $c_s(f)$. These velocities are increasing bounded functions, tending respectively towards $\overline{c}_{p1}$, $\overline{c}_{p2}$ and $\overline{c}_s$.

If the viscosity is neglected, the waves are purely propagated and the mechanical energy is constant. If $\eta \neq 0$, the fast wave is almost non-dispersive and non-diffusive. On the contrary, the slow wave becomes highly dispersive and diffusive. If $f \ll f_c$, then $c_{p2}(f) \ll \overline{c}_{p2}$: the slow wave tends towards a non-propagating mode [4]. The direct contribution of the slow wave to the overall wave propagation processes is therefore negligible. However, the accurate computation of the fast wave and of the shear wave depends crucially on the effects of the slow wave on the balance equations at interfaces.

3 Numerical modeling

3.1 Numerical scheme

To integrate (4), a uniform grid is introduced with spatial mesh size $\Delta\,x = \Delta\,y$ and time step $\Delta\,t$. A straightforward integration of (4) induces a condition of stability

$$\Delta\,t \leq \min\left(\frac{\Upsilon\,\Delta\,x}{\overline{c}_{p1}},\, \frac{2}{R(\mathbf{S})}\right), \tag{5}$$

where Υ is obtained by a Von-Neuman analysis of stability when $\mathbf{S} = \mathbf{0}$. In (5), the bound induced by the spectral radius of $\mathbf{S}$ is very restrictive. In sandstone saturated with water, for instance, the maximal CFL number is $\overline{c}_{p1}\,\Delta\,t/\Delta\,x \approx 10^{-2} \ll \Upsilon$. In sandstone saturated with bitumen, this number is roughly equal to 10^{-12}, preventing from practicable computations.

Here we propose a much more efficient strategy based on *Strang's splitting*, solving successively the propagative part

$$\frac{\partial}{\partial\,t}\,\mathbf{U} + \mathbf{A}\,\frac{\partial}{\partial\,x}\,\mathbf{U} + \mathbf{B}\,\frac{\partial}{\partial\,y}\,\mathbf{U} = \mathbf{0}, \tag{6}$$

and the diffusive part

$$\frac{\partial}{\partial\,t}\,\mathbf{U} = -\mathbf{S}\,\mathbf{U}. \tag{7}$$

The propagative part (6) is solved by an explicit ADER scheme [17], with a stencil of 25 nodes and $\Upsilon = 1$. This scheme leads to fourth-order of convergence, accounting for waves over long distances with small dispersion and diffusion errors, even on coarse grids: see [11] for a dispersion analysis. Since the physical parameters do not vary with time, the diffusive part (7) is solved exactly: p and σ are unchanged, whereas the velocities become ($i = 1,\, 2$)

$$\begin{aligned} &v_{si}^{n+1} = v_{si}^{n+1/2} + \frac{\rho_f}{\rho}\left(1 - e^{-\frac{\eta}{\kappa}\,\frac{\rho}{\chi}\,\frac{\Delta\,t}{2}}\right) w_i^{n+1/2}, \\ &w_i^{n+1} = e^{-\frac{\eta}{\kappa}\,\frac{\rho}{\chi}\,\frac{\Delta\,t}{2}}\,w_i^{n+1/2}. \end{aligned} \tag{8}$$

The splitting (6)-(7) with exact integration (8) recovers the optimal condition of stability: $\bar{c}_{p1}\,\Delta t/\Delta x \leq \Upsilon$. However, since $\mathbf{A}$ and $\mathbf{B}$ do not commute with $\mathbf{S}$, the order of convergence falls from 4 to 2. Higher-order splittings can be used, implying an additional computational cost [8].

3.2 Mesh refinement

The wavelength of the fast wave is much greater than that of the slow wave. Consequently, a uniform mesh size Δx leads to the following alternative: either a coarse grid well-suited to the fast wave is chosen, and the slow wave is badly discretized; either a fine mesh is used on the whole domain, and the computational cost which increases dramatically. Implementing a grid refinement only around the interface therefore provides an efficient approach.

Indeed, the incident waves are usually compressional or shear waves (see figure 2-(a)), generating the slow wave at the interfaces. The slow wave being crucial in the balance equations, a fine discretization inside the refined patch ensures accurate wave conversions. The diffracted fast compressional and shear waves propagated out of the refined zone are correctly computed on the coarse grid. The slow wave that goes out of the refined zone is badly discretized, but it is usually without importance: when viscous effects of the saturating fluid are non-negligible, the slow wave remains localized at the interface.

To limit the numerical dispersion on the coarse grid, it is preferable to also perform temporal refinement using a local CFL stability condition. Here we adopt an approach based on flux conservation [1], which is more naturally coupled to the flux-conserving scheme (6). The extrapolated values required to couple coarse and fine grids are obtained by performing linear interpolation in space and time on the numerical values at the surrounding nodes. If the mesh size of the fine grid is $\Delta x/q$, then q time substeps are necessary on this grid when one time iteration is done on the coarse one.

One must estimate carefully q to minimize the computational extra-cost. For that purpose, one computes the wavelengths $\lambda_1(f) = c_{p1}(f)/f$ and $\lambda_2(f) = c_{p2}(f)/f$ at the central frequency f of the source. The numbers of grid nodes per wavelength of the slow wave, in the fine grid, and of the fast wave, on the coarse grid, must be roughly equal, which provides $q(f) \approx c_{p1}(f)/c_{p2}(f)$.

3.3 Immersed interface method

Numerical modeling of poroelastic waves across interfaces requires some care, for three reasons. First, spurious diffractions are induced by a stair-step discretization of interfaces. Second, the jump conditions are not correctly enforced. Third and last, the smoothness requirement to solve (6) is not satisfied. To remove these drawbacks while maintaining the efficiency of cartesian-grid methods, we adapt an *immersed interface method* previously developed in acoustics and elastodynamics [12, 13, 11].

Technical details may be found in the aforementioned references; here, we recall only the basic principle of this numerical method. At the *irregular points* where the ADER's stencil crosses the interface Γ, the scheme (6) uses *modified values* of the solution, instead of the classical numerical values. The modified values are extrapolations, based on the local geometry of Γ and on k successive derivatives of the jump conditions (1). The integer k is called the *order* of the immersed interface method, and it plays a crucial role on its accuracy. Typically, a r-th order scheme requires at least order $k = r - 1$ to maintain the overall r-th order accuracy.

Since the jump conditions do not vary with time, the major part of the work can be done during a preprocessing step. At each time step, only a small number of matrix-vector products are involved. After optimization of the computer codes, the additional cost induced by the immersed interface method can be made negligible, lower than 1% of the computational time of the scheme.

4 Numerical experiments

Parameters	Ω_0	Ω_1
ρ_f (kg/m^3)	1040	985
η (Pa.s)	0	0
ρ_s (kg/m^3)	2650	2650
μ (Pa)	$1.85\,10^9$	$1.85\,10^9$
ϕ	0.3	0.2
a	2	2
κ (m^2)	10^{-12}	10^{-12}
λ_f (Pa)	$8.40\,10^9$	$4.84\,10^9$
β	0.88	0.56
m (Pa)	$7.05\,10^9$	$1.31\,10^{10}$
$\bar{c}_{p1}$ (m/s)	2364.9	1975.6
$\bar{c}_{p2}$ (m/s)	774.9	825.6
$\bar{c}_s$ (m/s)	960.4	914.4

Table 1: Parameters for the matrix (Ω_0) and for the scatterer (Ω_1).

4.1 A single scatterer

As a first experiment, we consider a circular scatterer of radius 30 m, centered in a computational domain of 300×300 m^2 discretized with $\Delta x = \Delta y = 1$ m. Around the cylinder, the mesh is refined with a factor $q = 4$ in the domain $[-40; 40]^2$ corresponding to 324×324 supplementary nodes. A second-order immersed interface method is used setting $k = 2$ in section 3.3. The physical parameters are detailed in table 1. The source is a right-going plane compressional fast wave, centered at 40 Hz (see figure 2 a-b). The CFL number is $\bar{c}_{p1}\,\Delta t/\Delta x = 0.95$. Refining with a factor $q = 4$ ensures roughly the same number of grid nodes per wavelength for the fast wave on the coarse grid and for the slow wave on the fine grid.

The simulations are performed on a single-processor computer at 2.2 GHz. Without mesh refinement, the immersed interface method involves 944 irregular points, leading to a preprocessing step of 18.5 s; each time iteration takes 0.28 s. With the fine grid, 3840 irregular

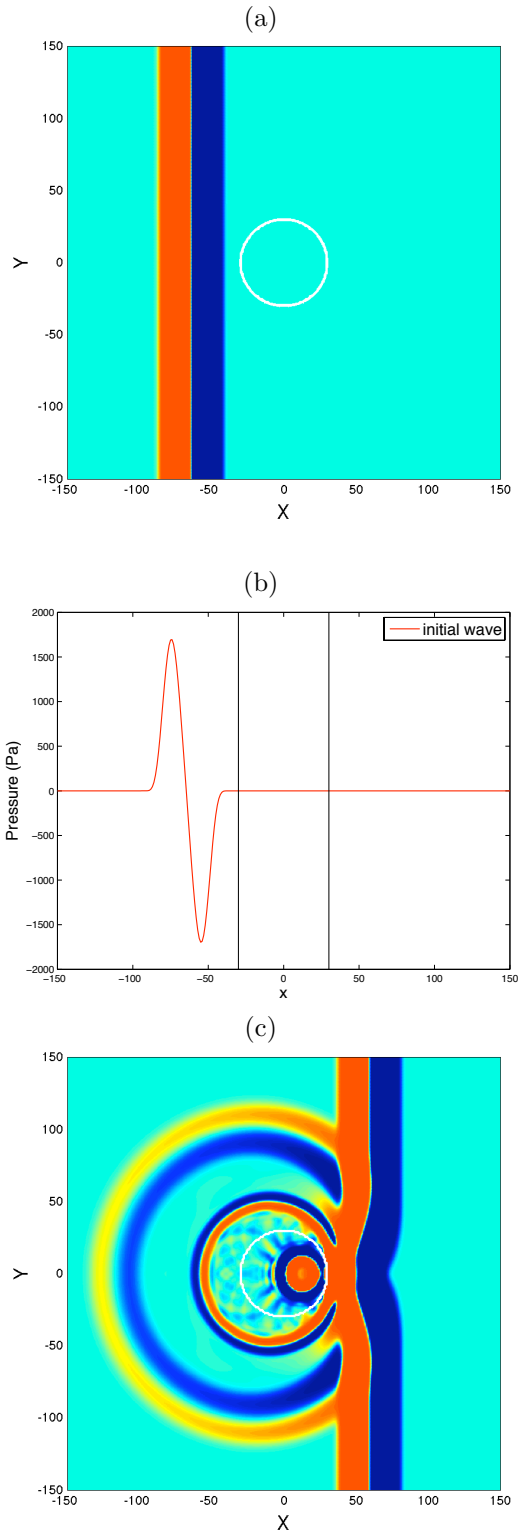

Figure 2: Plane wave impacting a circular scatterer. (a)-(b): pressure at initial time. (c): pressure after 130 time steps without interface method nor mesh refinement ($q = 1$ and $k = 0$).

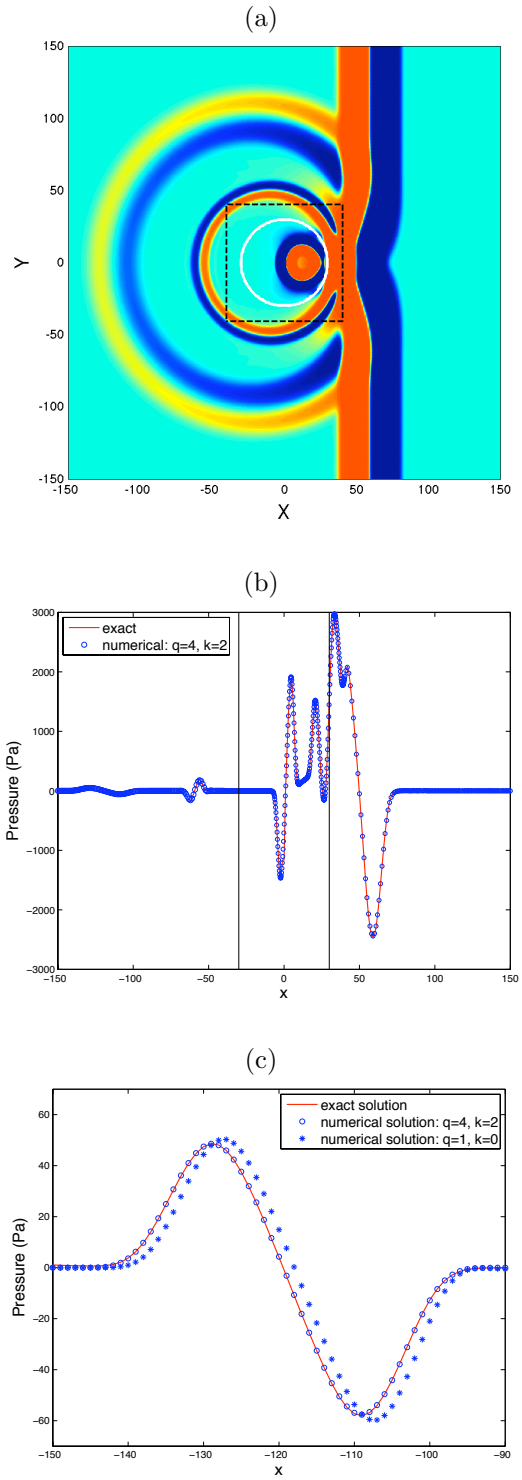

Figure 3: Plane wave impacting a circular scatterer: pressure after 130 time steps. Dashed area: refined zone. Slices at $y = 0$ m (b-c): numerical solution (blue circles) and exact solution (solid red line).

points are involved, and the previous times become respectively 71 s and 1.54 s: the increase of computational time is almost linear with q.

Figure 2(a-b) shows the pressure at initial time. On figure 2(c) we represente the pressure after 130 time steps, computed on a single coarse grid ($q = 1$) without immersed interface method ($k = 0$). Spurious numerical waves appear during the interaction with the cylinder and propagate through the domain.

On figure 3 the solution obtained with second order immersed interface method ($k = 2$) and mesh refinement ($q = 4$) is represented. On the cart (a), the refined zone is displayed as a dashed square. Slices are proposed at $y = 0$ m; the vertical lines denote the location of the interfaces. In (b), the numerical solution is compared with the exact solution computed with 2048

Fourier modes and 70 Bessel modes [11]. The agreement between exact and numerical solutions is very good.

A zoom around the reflected fast compressional wave in proposed in (c). The exact solution (solid line) is compared with the two previous numerical solutions presented in figures 2(c) and 3(a). The improvement introduced by the combination of interface method and local refinement is clearly visible. Without accurate treatment during the interaction, the fast compressional reflected wave is not accurately represented and is shifted compared with the exact solution.

4.2 Many scatterers

The numerical methods proposed along this paper are well-suited for non-academic configurations: complex geometries and multiple interfaces, where analytical methods fail. To illustrate the potential of our approach, we consider the interaction of a plane wave with three scatterers of various radii. Each cylinder is inside a patch refined four times, and second-order immersed interface method is implemented. The physical parameters are the same than in the previous test. Figure 4 displays the numerical solution at various instants. Such simulations enable numerical studies of the wave propagation in random poroelastic media [15].

5 Conclusion

Numerical modeling of 2-D transient Biot's model was addressed for waves whose frequency content lies in the low-frequency range. Three numerical tools were combined to obtain a method describing accurately the wave propagation: a fourth-order scheme with time-splitting; a space-time mesh refinement; and an immersed interface method. The resulting code provides highly-accurate simulations in realistic configurations.

The numerical experiments proposed in section 4 were done by assuming an inviscid saturating fluid. Nevertheless, the algorithms have been developped in view of the more general and penalizing case $\eta \neq 0$: see in particular section 3.1. Tests and comparisons with analytical solutions are in progress.

Since a fourth-order scheme is used, order $k = 3$ is theoretically required by the immersed interface method (section 3.3). The differentiations of jump conditions up this order are tedious, and need to be automatized. Note also that we have considered the interface between two poroelastic media in perfect bonded contact. Other configurations can be simulated: imperfect contacts, interfaces with vacuum or fluid, ... These cases will be the subject of further works.

As a last direction of work, let us mention the numerical modeling of transient Biot's equations in the full range of validity of poroelasticity. For frequencies greater than f_c in (2), a correction of the viscosity proportional with the square root of frequency needs to be introduced: see for instance the JKD model [10]. In the time domain, the evolutionary equations involve *fractional derivatives*, whose numerical evaluation is difficult and costly [14].

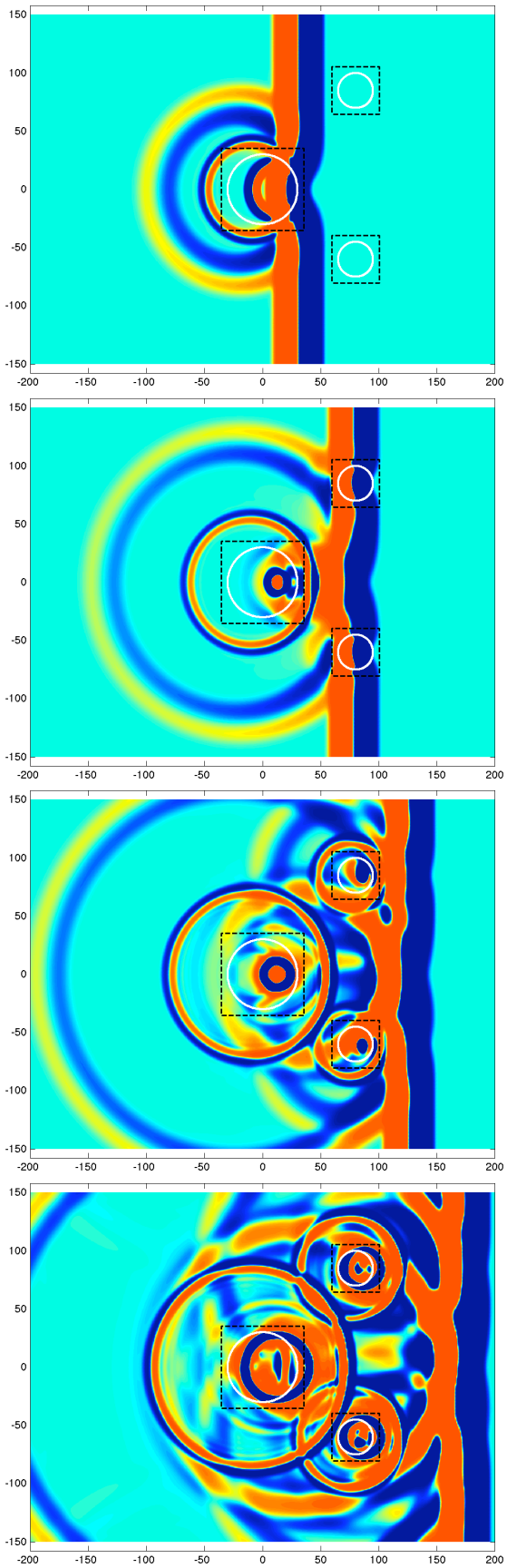

Figure 4: Plane wave impacting three scatterers: snapshots of the acoustic pressure p at successive instants. Dashed squares: refined zones.

References

[1] M. J. Berger, R. J. LeVeque, "Adaptative mesh refinement using wave-propagation algorithms for hyperbolic systems", *SIAM J. Numer. Anal.* 35-6, 2298-2316 (1998).

[2] M. A. Biot, "Theory of propagation of elastic waves in a fluid-saturated porous solid. I: Low-frequency range", *J. Acoust. Soc. Am.* 28-2, 168-178 (1956).

[3] M. A. Biot, "Theory of propagation of elastic waves in a fluid-saturated porous solid. II: High-frequency range", *J. Acoust. Soc. Am.* 28-2, 179-191 (1956).

[4] T. Bourbié, O. Coussy, B. Zinszner, "Acoustics of Porous Media", *Gulf Publishing Company* (1987).

[5] G. Chiavassa, B. Lombard, J. Piraux, "Numerical modeling of 1-D transient poroelastic waves in the low-frequency range", à paraître au *J. Comput. App. Math.* (2010).

[6] N. Dai, A. Vafidis, E. R. Kanasewich, "Wave propagation in heterogeneous porous media: a velocity-stress, finite-difference method", *Geophysics* 60-2, 327-340 (1995).

[7] A. Ezziani, Modélisation de la propagation d'ondes dans les milieux viscoélastiques et poroélastiques, PhD thesis, Université Paris-Dauphine (2005).

[8] E. Forest, R. D. Ruth, Fourth-order symplectic integration, *Physica D.* 43, 105-117 (1990).

[9] B. Gurevich, M. Schoenberg, "Interface conditions for Biot's equations of poroelasticity", *J. Acoust. Soc. Am.* 105-5, 2585-2589 (1999).

[10] D. L. Johnson, J. Koeplik, R. Dashen, Theory of dynamic permeability and tortuosity in fluid-saturated porous media, *J. Fluid. Mech.* 176, 378-402 (1987).

[11] B. Lombard, Modélisation numérique de la propagation et de la diffraction d'ondes mécaniques, HDR thesis, Université de la Méditerranée (2010).

[12] B. Lombard, J. Piraux, "Numerical treatment of two-dimensional interfaces for acoustic and elastic waves", *J. Comput. Phys.* 195-1, 90-116 (2004).

[13] B. Lombard, J. Piraux, "Numerical modeling of elastic waves across imperfect contacts", *SIAM J. Scient. Comput.* 28-1, 172-205 (2006).

[14] J. F. Lu, A. Hanyga, "Wave field simulation for heterogeneous porous media with singular memory drag force", *J. Comput. Phys.* 208, 651-674 (2005).

[15] F. Luppé, J. M. Conoir, S. Robert, "Coherent waves in a multiply scattering poro-elastic medium obeying Biot's theory", *Waves in Random and Complex Media* 18-2, 241-254 (2008).

[16] M. Schanz, "Application of 3-D time domain boundary element formulation to wave propagation in poroelastic solids", *Eng. Anal. Bound. Elem.* 25, 363-376 (2001).

[17] T. Schwartzkopff, M. Dumbser, C. Munz, "Fast high order ADER schemes for linear hyperbolic equations, *J. Comput. Phys.* 197-2, 532-539 (2004).

[18] Y. Q. Zeng, J. Q. He, Q. H. Liu, "The application of the perfectly matched layer in numerical modeling of wave propagation in poroelastic media", *Geophysics* 66-4, 1258-1266 (2001).

[19] C. Zhao, W. Li, J. Wang, "An explicit finite element method for Biot dynamic formulation in fluid-saturated porous media and its application to a rigid foundation", *J. Sound. Vib.* 282, 1169-1181 (2005).